2018 SCEC Annual Report

Characterizing Source Descriptions That Account for Nonlinear Effects in Linear Simulations

Report for SCEC Award 18190

PI: Dr. Kim B. Olsen

Institution: Department of Geological Sciences, San Diego State University, San Diego, CA 92182-1020

Publications and Reports:

Hu, Z., D. Roten, K.B. Olsen, and S.M. Day (2018). Kinematic Source Models for Earthquake Simulations with Fault-Zone Plasticity, *Seism. Res. Lett*. **89,** 2B, 806.

Hu, Z., D. Roten, K.B. Olsen, and S.M. Day (2018). Kinematic Source Models for Earthquake Simulations with Fault-Zone Plasticity, *SCEC Annual Mtg*, Sept 8-12, Palm Springs, CA, Poster #018,

Summary

Recent large-scale simulations (e.g., Roten et al., 2017; 2014) have shown that near-fault nonlinear (plastic) effects can reduce the ground motions by 50% or more, even at longer periods and at appreciable distance from the causative fault (such as in LA due to large events on the San Andreas fault, SAF). A main reason for this reduction is that Love waves are prevented from developing to otherwise large-amplitude phases by near-fault plastic effects. We have implemented and tested a novel and efficient approach to account for nonlinear/plastic effects in CyberShake with its current adjoint, linear framework. We first characterize first-order differences in slip, peak sliprate, and shape of the source time function due to near-fault plastic effects. Then, we implement the source description into AWP and verify that the ground motions produced by the linear simulations are sufficiently close to those produced by the equivalent nonlinear simulations.

Completed Work

We have set up a number of dynamic simulations using the AWP-ODC 3D finite-difference code, including Drucker-Prager plasticity. Specifically, we performed dynamic simulations up to 1 Hz of an *M* 7.8 earthquake scenario rupturing the southern San Andreas Fault, based on the model used in Roten et al. (2017). The planar fault was embedded in a 3-D heterogeneous velocity mesh (SCEC CVM4, Magistrale et al. 2000) with a 450-m wide low-velocity zone, where shear wave amplitudes are reduced by 30%.

The reduction of shear strength is described by the generalize Hoek-Brown failure criterion (Hoek et al., 2002), which uses a reduced value m_b evaluated from the Geological Strength Index (GSI) of the rock. The value of GSI ranges from 0 to 100, related to the degree of fracturing and weathering of rock. A larger GSI value indicates less disturbed rock, while for example, a low GSI value of 30 represents a heavily broken rock. The Hoek-Brown model is used to approximate the curved Hoek-Brown failure criterion and derive the equivalent cohesions and friction angles for two different rock models, sandstone and shale, with GSI values of 50 and 30, respectively.

We performed dynamic rupture simulations for several different realizations of the random stress field and selected a representative case for different media. In the linear case, surface PSRs are about 7 m/s for most parts of the fault and reach peak values (> 14 m/s) in the right portion of the fault. These surface PSR values are reduced to less than 4 m/s in the non-linear simulation for the sandstone model, and even less for the shale model. Note, that he rupture above the nucleation zone in the non-linear cases fail to reach the surface. The overall reduction in PSRs is most pronounced in the shallow zone, which is consistent with Roten et al. (2014).

Peak Slip Rate–Depth Profile

Since permanent deformation concentrates near the fault, we assume that plastic yielding of crustal rock in the fault zone produces the majority of the differences in ground motions. Figure 2 compares slip rates between linear and non-linear simulations along depth. The linear models excite high PSRs near the surface (above 3 km), which can be as large as two times of the PSRs for sandstone models on the surface. On the other hand, both models generate almost identical PSRs in the deeper part of the fault. The ratio of PSRs between non-linear and linear models gradually increase from about *0.4*-0.5 at the surface to close to 1 near the bottom of the fault.

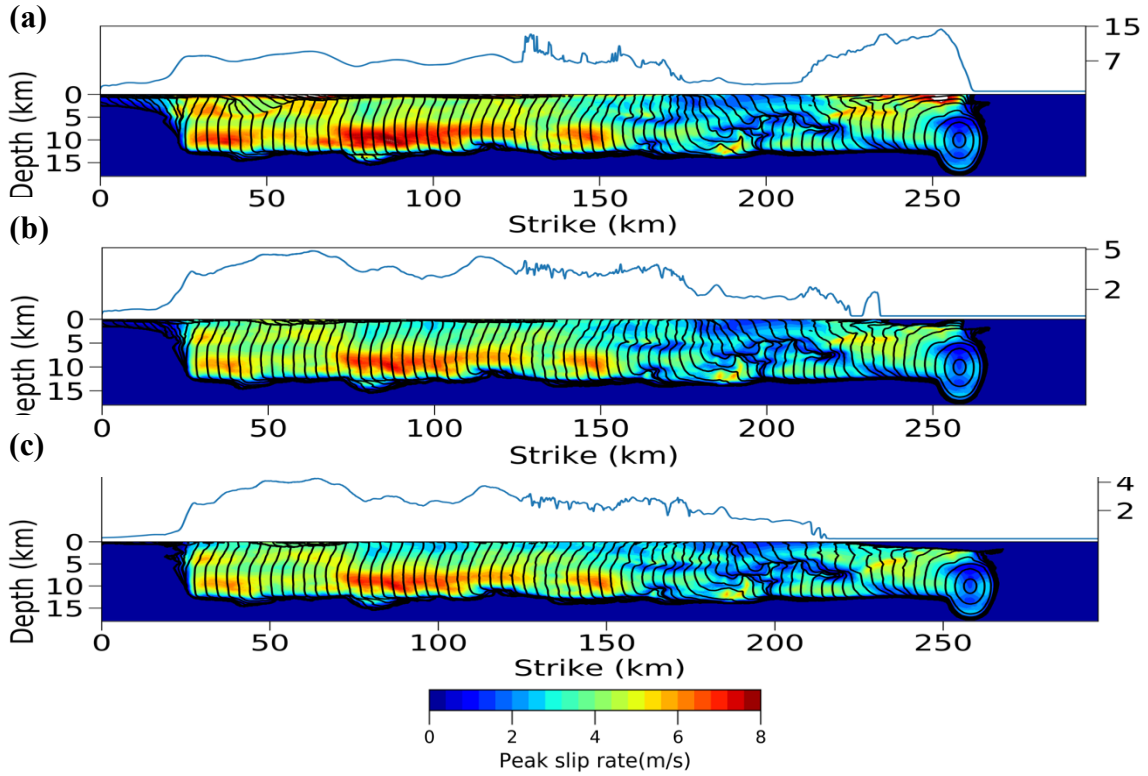

Figure 1. Peak slip rate distribution on the fault from a representative model, with the surface peak slip rate shown in blue above each subplot. (a) Linear; (b) sandstone; and (c) shale model. Black contours indicate rupture time in 1 s intervals.

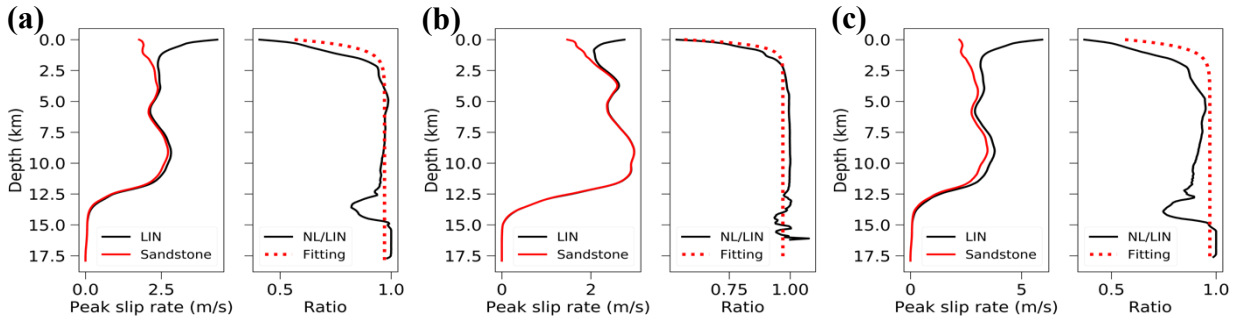

Figure 2. Average peak slip rate profile along depth (left panel of each subplot) for a sandstone nonlinear and a linear model, as well as the ratio between them (right panel of each subplot). (a)-(c) are three realizations for the sandstone model with stress drops of 7, 8, and 10 MPa, respectively. The dashed red line indicates the best fitting curve for the ratio profile.

The consistent pattern of the PSR ratio profiles motivates the idea to design a fitting curve, which modifies the linear PSR profile to mimic the non-linear PSR profile, and therefore producing similar resulting ground motions. We adopted the fitting curve with the formula,

$$r_{fit} = A + B * \exp\left(f_{depth}\right), \tag{1}$$

and regression of many realizations gives a best-fit function,

$$r_{fit} = 0.97 + \left(0.97 - \frac{GSI}{100}\right) * \exp\left(\frac{depth}{d_{norm}}\right), \tag{2}$$

where d_{norm} is a normalized depth, above which the reduction of PSRs in non-linear cases becomes pronounced. We approximated d_{norm} using the depth where the PSR profile for the linear model first turns flat. The fitting curve above is therefore only a function of depth and rock strength (represented by GSI values).

Kinematic Source Model

As mentioned above, fault-zone plasticity reduces slip rates on the fault. Given any source time function (STF) for a linear model, its corresponding non-linear PSR-depth profile can be retrieved by multiplying the fitting curve with the linear PSR profile. The plastic yielding primarily occurs when strain is large, so the most significant difference in STF between non-linear and linear models occurs in a small portion around the failure time. We therefore multiply the STF on each subfault with a conversion function, whose peak time is identical with that of the STF for the linear model, and the minimum value is the fitting curve value at the depth of the subfault. The process to modify a STF to obtain the converted STF is shown in Figure 3. The modification is applied to all subfaults and generates an equivalent kinematic source (EKS) model. Since the converted STF is very close to that for the non-linear model, it is reasonable to expect that the EKS model is able to reproduce similar ground motions with the non-linear model.

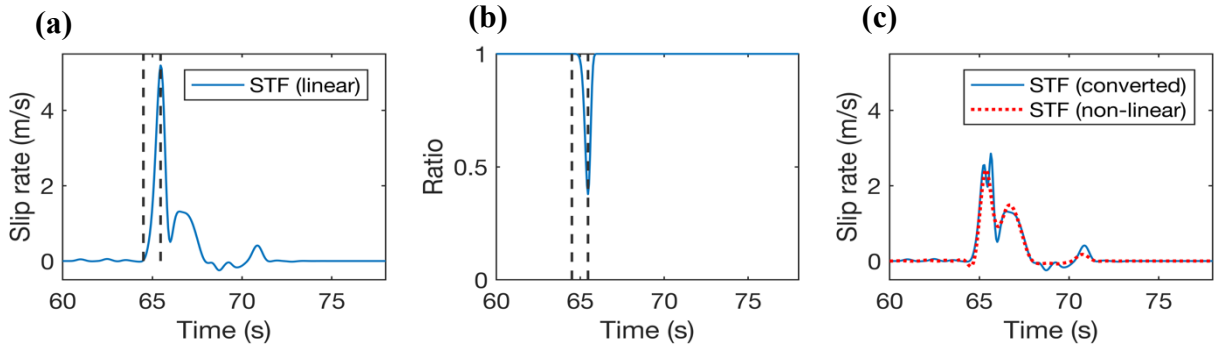

Figure 3. The STF on a representative subfault (depth=0) for the linear model (left), the non-linear model and modified STF (right). The middle figure shows the conversion function with a minimum value of 0.38, which is exactly the value of the fitting curve on the surface. The black dashed lines in the left and middle figure indicate peak time of the STF and conversion function.

Comparison of Ground Motions

Figure 4 shows peak ground velocities for a representative realization with three different models. In the linear case, strong shaking (PGV>3 m/s) occurs near the fault; some small patches of strong ground motions (PGVs larger than 1.5 m/s) also appear in the Los Angeles (LA) Basin and Oxnard. These patterns have been reported in previous simulations and confirmed by ambient noise measurements (Denolle et al., 2013, 2014), which can be attributed to wave guide effects. The non-linear model predicts significant smaller PGVs near the fault, where PGVs are reduced to about 2 m/s and 1 m/s and smaller. The reduction is relatively less pronounced in the areas near the fault. Compared with the linear model, the EKS model produces weaker shaking, similar to that from the non-linear models, although the reduction level is smaller.

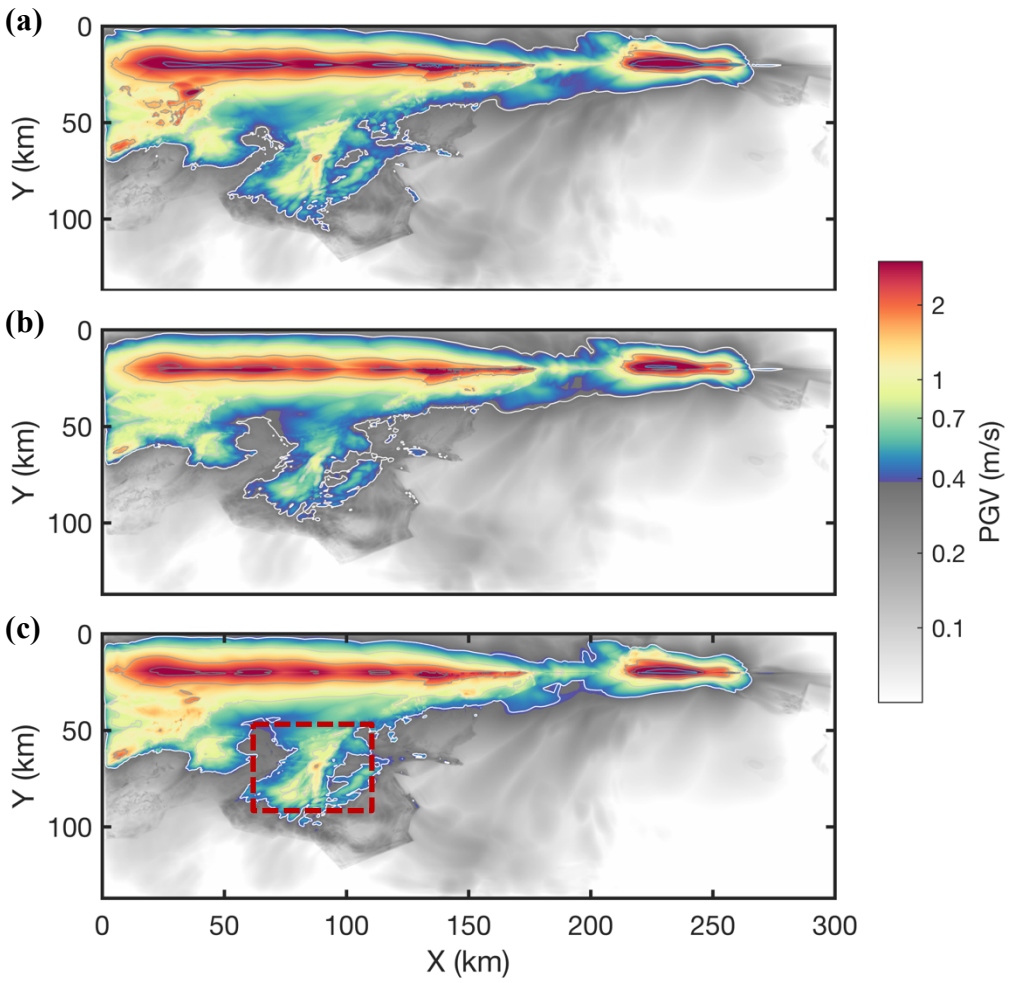

Figure 4. PGV distribution for the southern San Andreas Fault region, obtained for (a) linear, (b) sandstone and (c) the EKS model. Contour lines are added for clarity. The red dashed rectangle shows the LA basin region used in Figure 6.

Reduction of Ground Motion Extremes

The non-linearity also affects ground motion extremes, for which we computed the cumulative distribution of PGVs (Figure 5). Plastic effects reduce the amplitude and occurrence of strong ground motions, e.g. at an occurrence frequency of 10^{-4} PGVs decrease from 4.5 m/s in the linear simulation to 3.5 m/s in the non-linear simulations, which is well reproduced in the EKS model. The results are consistent for sandstone and shale, while shale generates slightly more reduction than sandstone due to its lower strength.

We also computed the distribution of spectral acceleration at 3s (3s-SA, 5) to analyze the effects of plasticity and efficacy of the EKS model at different frequencies. The distribution pattern of 3s-SA is similar with that of the PGVs, except that non-linearity reduces infrequent 3s-SAs up to 40-50%, larger than the reductions for PGVs.

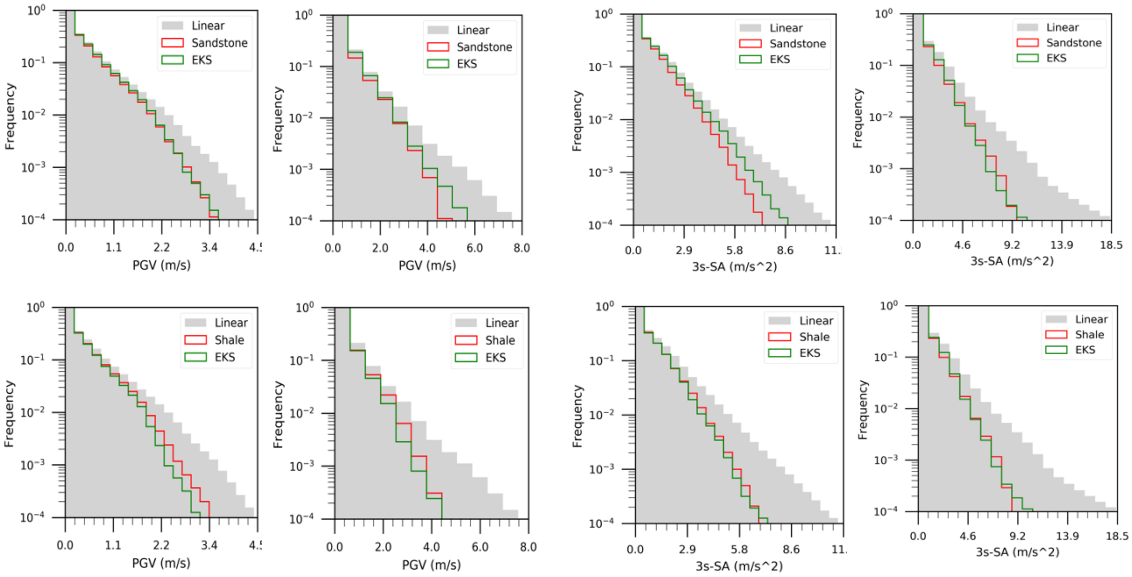

Figure 5. Cumulative distribution of (left two columns) PGVs and (right two columns) SA-3s for the 3 different models. The left and right columns for both PGVs and SAs are from two models with different stress drop (7 and 10 MPa, respectively). The top row is for the non-linear model with sandstone, the bottom for shale.

Regions far away from the Fault

Even though the EKS model can reproduce similar overall ground motion reduction features with non-linear models, the reduction in regions away from the fault remains a challenge. As shown in Figure 4, some strong motion patches exist in the EKS model, where the non-linear model show smaller ground motions. Figure 6 shows histograms of the PGVs for three models in the LA basin. For the shale media, the EKS model works quite well to produce the PGV distribution patterns that are consistent with non-linear models, whereas the EKS model overpredicts the PGVs for the sandstone model. This may be explained by the fact that the sandstone model generates PGVs in the LA basin comparable with those from the shale model, instead of stronger shaking due to greater rock strength and less inelastic absorption of seismic energy.

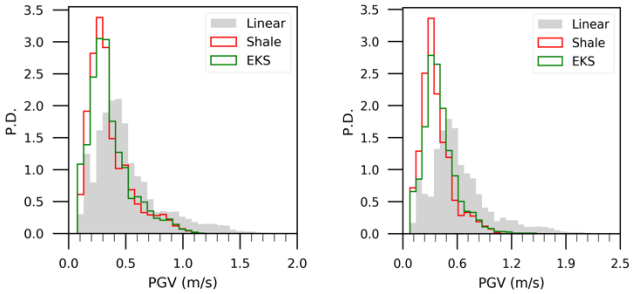

Figure 6. Histograms of PGVs in the area around the LA basin. The models are the same as Figure 5.

Future Work

The EKS models proposed here only depend on rock strength and depth. Dependency on factors including initial stress, stress drop, earthquake magnitude should be tested in the future, including more simulations with different realizations of these parameters, including non-surface-rupturing scenarios.

References

Denolle, M. A., E. M. Dunham, G. A. Prieto, and G. C. Beroza (2013). Ground motion prediction of realistic earthquake sources using the ambient seismic field, J. Geophys. Res. Solid Earth, vol 118, pp. 2102–2118, doi:10.1029/2012JB009603.

Denolle, M. A., E. M. Dunham, G. A. Prieto, and G. C. Beroza (2014). Strong ground motion prediction using virtual earthquakes, Science, vol 343, pp. 399–403, doi:10.1126/science.1245678.

Hoek, E., Corkum, B., Carranza-torres, C. & Corkum, B. Hoek-Brown failure criterion. *NARMS-TAC Conf. Toronto* (2002). doi:10.1016/0148-9062(74)91782-3.

Magistrale, H. The SCEC Southern California Reference Three-Dimensional Seismic Velocity Model Version 2. *Bull. Seismol. Soc. Am.* (2000). doi:10.1785/0120000510.

Roten, D., Olsen, K. B., Day, S. M., Cui, Y. & Fäh, D. Expected seismic shaking in Los Angeles reduced by San Andreas fault zone plasticity. *Geophys. Res. Lett.* **41,** 2769–2777 (2014).

Roten, D., Olsen, K. B. & Day, S. M. Off-fault deformations and shallow slip deficit from dynamic rupture simulations with fault zone plasticity. *Geophys. Res. Lett.* **44,** 7733–7742 (2017).